Iowa Research Online
The University of Iowa's Institutional Repository

University of Iowa
Iowa Research Online

Theses and Dissertations

2010

Lidar measurement of boundary layer evolution to determine values of the entrainment coefficient A

Heather Amanda Cross
University of Iowa

Copyright 2010 Heather Amanda Cross

This dissertation is available at Iowa Research Online: http://ir.uiowa.edu/etd/482

Recommended Citation
Cross, Heather Amanda. "Lidar measurement of boundary layer evolution to determine values of the entrainment coefficient A." MS (Master of Science) thesis, University of Iowa, 2010.
http://ir.uiowa.edu/etd/482.

Follow this and additional works at: http://ir.uiowa.edu/etd

Part of the Civil and Environmental Engineering Commons

LIDAR MEASUREMENT OF BOUNDARY LAYER EVOLUTION TO DETERMINE VALUES OF THE ENTRAINMENT COEFFICIENT A

By

Heather Amanda Cross

A thesis submitted in partial fulfillment of the requirements for the Master of Science in Civil and Environmental Engineering (Water Resources) in the Graduate College of The University of Iowa

May 2010

Thesis Supervisor: Professor William Eichinger

Graduate College
The University of Iowa
Iowa City, Iowa

CERTIFICATE OF APPROVAL

MASTER'S THESIS

This is to certify that the Master's thesis of

Heather Amanda Cross

has been approved by the Examining Committee for the thesis requirement for the Master of Science degree in Civil and Environmental Engineering (Water Resources) at the May 2010 graduation.

Thesis Committee: _____
William Eichinger, Thesis Supervisor

_____
Allen Bradley

_____
Keri Hornbuckle

ABSTRACT

The Soil Moisure-Atmosphere Coupling Experiment (SMACEX) was conducted as part of the larger Soil Moisture Experiments (SMEX) field campaign in the Walnut Creek watershed near Ames, Iowa over the period from 15 June to 11 July 2002. As part of that work, measurements of the height of the boundary layer were gathered using a vertically staring lidar, and a method was developed for calculating the value of the entrainment parameter, A, from boundary layer geometry. The entrainment heat flux is of major importance to boundary layer models, representing the amount of energy that is supplied to the boundary layer by entrainment from the air above, which contributes to the growth of the boundary layer. The entrainment parameter, A, is defined as the ratio of the virtual potential temperature heat fluxes at the surface and at the top of the boundary layer. Most of the suggested values of A range between 0.1 and 0.3, with A=0.2 considered to be a good average to use in most modeling.

In this paper we calculate the value of the entrainment parameter A based on entrainment zone geometry and examine a relationship between the entrainment parameter A, the vertical potential temperature gradient, and boundary layer development. The results here indicate that during some periods of boundary layer growth, the entrainment coefficient does not maintain a constant value. It is a characteristic that changes depending on the stage of boundary layer evolution.

TABLE OF CONTENTS

LIST OF TABLES iv

LIST OF FIGURES v

LIST OF SYMBOLS vi

LIST OF ACRONYMS vii

INTRODUCTION 1

CHAPTER

1. ATMOSPHERIC BOUNDARY LAYER MODEL 6
2. EXPERIMENT SITE AND EQUIPMENT 10
3. METEOROLOGICAL MEASUREMENTS 15
4. LIDAR DATA ANALYSIS METHODOLOGY 19
5. DISCUSSION 23

CONCLUSION 31

REFERENCES 33

LIST OF TABLES

Table 1. Operating characteristics of the vertically staring lidar system. 13

LIST OF FIGURES

Figure 1.	A traditional thermodynamic model of an unstable atmospheric boundary layer (Stull 1988).	3
Figure 2.	A black-and-white aerial photograph of the field campaign site showing a bare-soil condition.	11
Figure 3.	A photograph of the vertically staring lidar.	12
Figure 4.	An example of two hours of lidar boundary layer data from 29 June, 2002.	14
Figure 5.	Radiosonde profiles from 27 Jun 2002.	15
Figure 6.	June 25, 2002, 0658 and June 29, 0707.	16
Figure 7.	A photograph of SMEX field campaign team members launching a Vaisala meteorological balloon.	18
Figure 8.	A photograph of the CSAT3 and LI7500 station.	18
Figure 9.	An example of a lidar scan showing the top of the boundary layer and the values for the edge-detection function (blue line), and the lidar signal showing the decrease in aerosol concentration at the top of the boundary layer (solid line).	20
Figure 10.	The calculated values of the entrainment parameter A are plotted against the vertical potential temperature gradient corresponding to boundary layer height.	24
Figure 11.	Figure 5 from Nelson et al (1989) showing the evolution of normalized entrainment zone depth (Δh) with entrainment velocity (w_e) for 15 June 1983 at the BLX83 field site in Oklahoma.	25
Figure 12.	A sampling of the June 27 temperature profile showing two distinct regions of boundary layer development close to the earth's surface.	27
Figure 13.	The calculated values of the entrainment parameter A are plotted against the vertical temperature gradient.	28

LIST OF SYMBOLS

A	entrainment parameter
B	parameterization constant with commonly accepted values of 2.5
C	parameterization constant with commonly accepted values of 8
dh/dt	growth rate of the boundary layer
dT/dH	change in temperature with change in height
g	acceleration resulting from gravity
h	height of the boundary layer
h_{bottom}	height of the bottom of the entrainment zone
h_{top}	height of the top of the entrainment zone
k	von Kármán constant
L	Monin-Obukhov length
t	time
T	temperature of the boundary layer
u^*	friction velocity
σ	variance
w_s	subsidence velocity
$\overline{w'\theta'}_{surface}$	sensible heat flux at the surface
γ	potential temperature gradient above the boundary layer

LIST OF ACRONYMS

ABL	atmospheric boundary layer
APD	avalanche photodiode
BLH	boundary layer height
CDT	central daylight time
EZ	entrainment zone
EZT	entrainment zone thickness
LST	local sidereal time
PC	personal computer
SMACEX	Soil Moisture-Atmosphere Coupling Experiment
SMEX	Soil Moisture Experiment
UI	The University of Iowa

INTRODUCTION

Air quality modeling at the local or regional scale is required for a variety of purposes and can be carried out using a wide variety of models. Substances emitted into the atmospheric boundary layer (ABL) are gradually dispersed horizontally and vertically through the action of turbulence, and eventually become completely mixed over this layer if sufficient time is available and if there are no significant sinks. The height, *h*, of the boundary layer (also commonly called the mixing, or mixed layer) is a key parameter for air pollution models. It determines the volume available for the dispersion of pollutants and is involved in many predictive and diagnostic methods and/or models to assess pollutant concentrations. It is also an important parameter in atmospheric flow models. There has not been a great deal of research on the growth of the boundary layer. Its height is often an unspecific parameter lacking a straightforward definition or method of estimation. It is a phenomenon that occurs at heights of about a kilometer, where conventional surface instruments cannot reach. Remote sensors, like lidar, can provide some information, but not a complete description of the meteorological conditions. One of the key assumptions used in modeling the growth of the boundary layer is the amount of energy entrained into the boundary layer from the free atmosphere as it rises. This quantity is required to compute the transport, dispersion and removal of pollutants. The dispersion of pollutants depends in part on this rate of growth and from the other meteorological parameters determined as a result of that growth (Seibert et al 1998).

The boundary layer can be defined as the part of the troposphere which is directly influenced by the presence of the earth's surface on time scales of about one hour (Stull, 1988). The thickness or depth of the boundary layer is

determined in large part by the buoyancy produced when solar energy is absorbed by the earth's surface and transferred to the air above the surface. Additional energy is transferred to the boundary layer from the air above in the transition region between the boundary layer and the free atmosphere, called the entrainment zone (EZ, see Figure 1). The well-mixed portion of the boundary layer below the EZ is called the mixed layer. Understanding the physical processes that influence the growth of the boundary layer is important for a number of applications including air quality, weather prediction, climate, agriculture, and water resources.

The depth of the boundary layer is a complex function that varies each day in accordance with the availability of solar energy. As solar energy heats the earth each day, heat energy is transported from the earth's surface to the air just above, warming it. This warm air is buoyant, causing it to rise up into the boundary layer, with the result that the boundary layer grows in height and warms. The height to which these plumes rise is determined by a stable capping inversion in which the temperature of the ambient air increases with height. The system reaches equilibrium when the warm air parcel from the surface reaches the altitude where the temperature of the parcel and the temperature of the ambient air are equal. However, the vertical motion of the air parcel gives it kinetic energy so that these buoyant thermal plumes rising within the mixed layer over-shoot this equilibrium position and move higher into the capping stable air above before sinking back into the mixed layer. These air parcels experience some oscillation about the equilibrium height. Associated with this overshoot process, is the entrainment of air from the free atmosphere above, downward into the boundary layer (Nelson et al, 1989). The equilibrium height is the height of the boundary layer. The motion of boundary layer air above the boundary layer height and the

subsequent entrainment of free atmosphere air into the boundary layer causes an area in which there exists both air from above and air from below; this is the entrainment zone. In order to measure and predict transport processes within the boundary layer, it is important to understand how boundary layer growth is influenced by the entrainment of air from the free atmosphere.

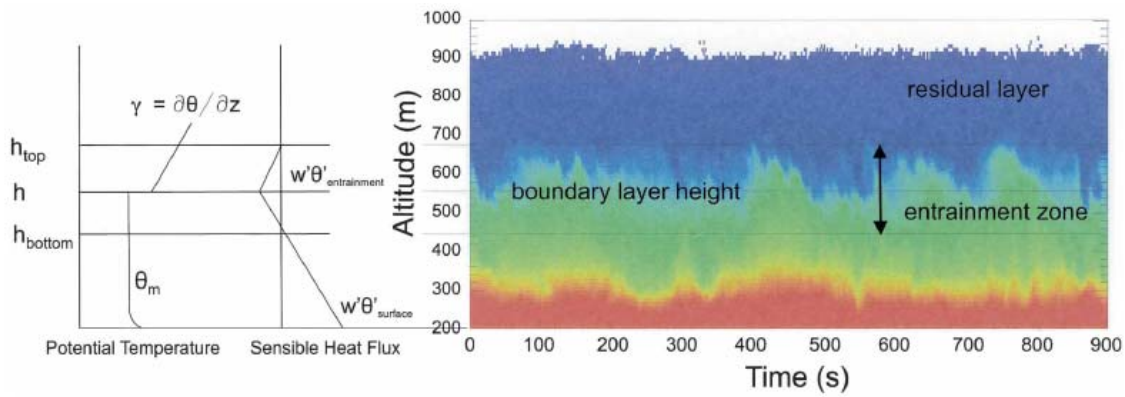

Figure 1. A traditional thermodynamic model of an unstable atmospheric boundary layer (Stull, 1988). A logarithmic layer near the surface blends into a constant temperature mixed layer that extends to the top of the boundary layer. A stable atmosphere with a temperature inversion acts as a lid to the vertical motions of the air below. A lidar signal showing the height of the boundary layer with time is shown on the right. Reds are highest particulate concentrations and blues are lowest. The thermodynamic diagram is shown to the left scaled to the lidar signal.

The entrainment heat flux is of major importance to boundary layer models, representing the amount of heat energy that is supplied to the boundary layer by entrainment from the air above, which contributes to the growth of the boundary layer. Conventional estimates put the amount of energy that comes from above at about 20 percent of the total. An entrainment parameter, *A*, is defined as the ratio of the virtual potential temperature heat fluxes at the surface and at the top of the boundary layer (Stull 1988).

There have been a number of studies that have attempted to measure the entrainment parameter A. Laboratory experiments and some observational studies have shown the ratio to be approximately $A \approx 0.2$ for thermally driven, dry convective boundary layers (Stull 1976, 1988; Nicholls and LeMone 1980). Most of the suggested values of A range between 0.1 and 0.3, with A=0.2 considered to be a good average to use for free convection (Stull, 1976a). Many authors use A=0.2 as a typical value (e.g., Tennekes, 1973; Yamada and Berman, 1979; Driedonks, 1982b). More complicated models that include the mechanical generation of turbulence or forced convection (Mahrt and Lenschow 1976; Zeman and Tennekes 1977; Smeda 1979; Driedonks 1982a), and more recent studies (Betts et al. 1990, 1992; Culf 1992; Betts and Ball 1994, 1995, 1998; Betts and Barr 1996; Davies et al. 1997; Angevine 1999; Margulis and Entekhabi 2004), have found values of this entrainment parameter to be significantly larger ($A \approx 0.4$) for windy conditions. Recent comparisons with measurements from different climatic regions also suggest the higher typical value of A=0.4 (e.g., Tennekes and van Ulden, 1974; Clarke, 1990; Betts, 1992; Culf, 1992). Conventional atmospheric modeling assumes the entrainment parameter to be a constant. This is equivalent to fixing the ratio of the amount of energy contributed from the free atmosphere towards the development of the boundary layer.

Previous work by Eichinger et al. (2005) estimated the regional sensible heat flux from measured values of the boundary layer height by inverting a method of estimating the height of the boundary layer (Batchvarova and Gryning 1991; Gryning and Batchvarova 1994). As part of that work, a method was outlined for calculating the entrainment parameter A based on the entrainment zone thickness and the height of the boundary layer. Because of the key role that the entrainment parameter plays in atmospheric

modeling, it is fortunate that it can be expressed in terms of the physical size and shape of the top of the boundary layer, which can be measured directly by lidar.

The data used for this study were taken during the month of June 2002 as part of the Soil Moisture–Atmosphere Coupling Experiment (SMACEX). SMACEX was conducted as part of the larger Soil Moisture Experiment (SMEX) field campaign. The test area used in this work was just south of Ames, Iowa.

In this study we will calculate the value of the entrainment parameter A based on entrainment zone geometry and examine a relationship between the entrainment parameter A, the vertical potential temperature gradient, and boundary layer development.

CHAPTER 1

ATMOSPHERIC BOUNDARY LAYER MODEL

The Batchvarova and Gryning model (1991, 1994, hereafter Batchvarova–Gryning model) is a one-dimensional approach to the growth of an inversion–capped atmospheric boundary layer (ABL) originally developed by Betts (1973), Carson (1973), Tennekes (1973), and Zilitinkevich (1975) (Figure 1). The Carson and Tennekes model and its more simplified forms have been the basis for nearly all of the boundary layer height models that have been developed. The Batchvarova–Gryning model uses a parameterization of the turbulent kinetic energy budget within the mixed layer. This assumes that the turbulence within the mixed layer is sufficiently strong to maintain a layer of nearly uniform potential temperature distribution and that the mixed layer is capped by a sharp potential temperature jump (Batchvarova and Gryning, 1994).

According to the Batchvarova–Gryning model, the relationship between the sensible heat flux at the surface $\overline{w'\theta'}_{surface}$, the height of the boundary layer *h*, and the other surface parameters is

$$\frac{\overline{w'\theta'}_{surface}}{\gamma} = \left[\frac{h^2}{(1+2A)h - 2BkL} + \frac{Cu*^2\,T}{\gamma g(1+A)h - BkL}\right] \times \left[\frac{dh}{dt} - w_s\right] \quad (1)$$

where dh/dt is the growth rate of the boundary layer, *t* is time, *L* is the Monin–Obukhov length, *k* is the von Kármán constant, *g* is the acceleration resulting from gravity, *u** is the friction velocity, *T* is the temperature of the

boundary layer, γ is the potential temperature gradient above the boundary layer, and w_s is the subsidence velocity; B and C are normally taken to be parameterization constants with commonly accepted values of 2.5 and 8, respectively (Melas and Kambezidis 1992; Gryning and Batchvarova 1996; Källstrand and Smedman 1997; Steyn et al. 1999). For this study, the subsidence velocity, w_s will be neglected. Until the boundary layer reaches its maximum height, the remnants of boundary layer (the residual layer) from the previous day can be seen by the lidar. If the subsidence velocity is non-zero, the top of the residual layer will decrease in height. The selected days were chosen based in part on a residual layer that did not change altitude, so $w_s = 0$.

As stated previously, the ratio of the entrainment sensible heat flux (from the entrainment of warm air above the inversion into the boundary layer) to the surface sensible heat flux is A. This quantity can be obtained directly from the lidar data. A is defined to be the ratio of the potential temperature fluxes as

$$A = -\frac{\overline{w'\theta'}_{ventrainment}}{\overline{w'\theta'}_{vsurface}} \approx \frac{\overline{w'\theta'}_{entrainment}}{\overline{w'\theta'}_{surface}} \quad (2)$$

Knowing that the virtual heat flux is zero near the bottom of the entrainment zone and that the entrainment flux is a maximum at the average height of the boundary layer, and assuming linear changes in the heat fluxes with height (Figure 1), A can be expressed in terms of the dimensions of the boundary layer (Davies et al. 1997). This relationship is written as

$$A = \frac{h}{h_{bottom}} - 1 = \frac{EZT}{2h - EZT} \quad (3)$$

where h_{bottom} is the height of the bottom of the entrainment zone and EZT is the entrainment zone thickness (h_{top} - h_{bottom}).

The first term on the right-hand side of Eq. (1) represents the growth of the boundary layer resulting from sensible heat flux from the surface and to the entrainment of warm air from above the boundary layer. The second term is the Zilitinkevich correction, which incorporates the contribution to mixed-layer growth resulting from the mechanical mixing of the air near the surface (Zilitinkevich 1975). Early in the morning, when the atmosphere is near neutral and buoyancy is not important, the growth rate of the shallow mixed layer is proportional to the friction velocity. As the boundary layer grows, buoyancy becomes increasingly important. Mechanical turbulence at the surface ceases to be important when the boundary layer has grown to a height of approximately -1.4 L (Gryning and Batchvarova 1990) where L is the Obukov length (Stull, 1988). Because the lidar, as configured during the field campaign, has a minimum altitude of 120 m, the only conditions that can be observed are those in which the Zilitinkevich correction is small (less than 2% contribution). Accordingly, the second term has been ignored. Thus, this method is not appropriate for use in the very early morning, when mechanical turbulence is important. Further, the method is useful only during that period when the boundary layer is growing (until approximately solar noon). This is because h and dh/dt are the primary measures used to estimate the amount of energy that has been added to the boundary layer.

Once the boundary layer has grown to its maximum height, or has risen to the height of the cumulus cloud bottom, the method cannot be applied.

CHAPTER 2

EXPERIMENT SITE AND EQUIPMENT

SMACEX was conducted in the Walnut Creek watershed near Ames, Iowa, over the period from 15 June to 11 July 2002. The surface cover during the time of this experiment was a mix of immature corn and soybean fields, in the upwind direction. The size of an individual field along the wind direction ranged from 300 to 800 m. A main focus of SMACEX is the investigation of the interactions between the atmospheric boundary layer, surface moisture, and canopy (Kustas et al. 2005). Figure 2 is an aerial photograph of the site taken during a period with little or no vegetation. The patchiness of the photograph is indicative of the small variations in height (1–4 m) in the field. A vertical sounding elastic lidar was located at the boundary between a corn and a soybean field. During the field campaign, the lidar operated daily during daylight hours.

The lidar used for this analysis is a portable, vertically staring lidar system; it is pictured in Figure 3. The basic parameters of the transmitter and receiver of the University of Iowa (UI) vertically staring lidar system are given in Table 1. The system uses a Nd:YAG laser operating at 1.064 μm. The laser pulse is 10 ns long, with a beam divergence of approximately 3 mrad. The laser pulse energy is a maximum of 125 mJ with a repetition rate of 50 Hz. The receiver telescope is a 25-cm, f/10, commercial Cassegrain telescope. The light is focused to the rear of the telescope where it passes through a 3-nm-wide interference filter and two lenses, which focus the light onto a 3-mm, IR-enhanced, silicon avalanche photodiode (APD). An iris, located just before the APD, serves as a stop to limit the field of view of the telescope.

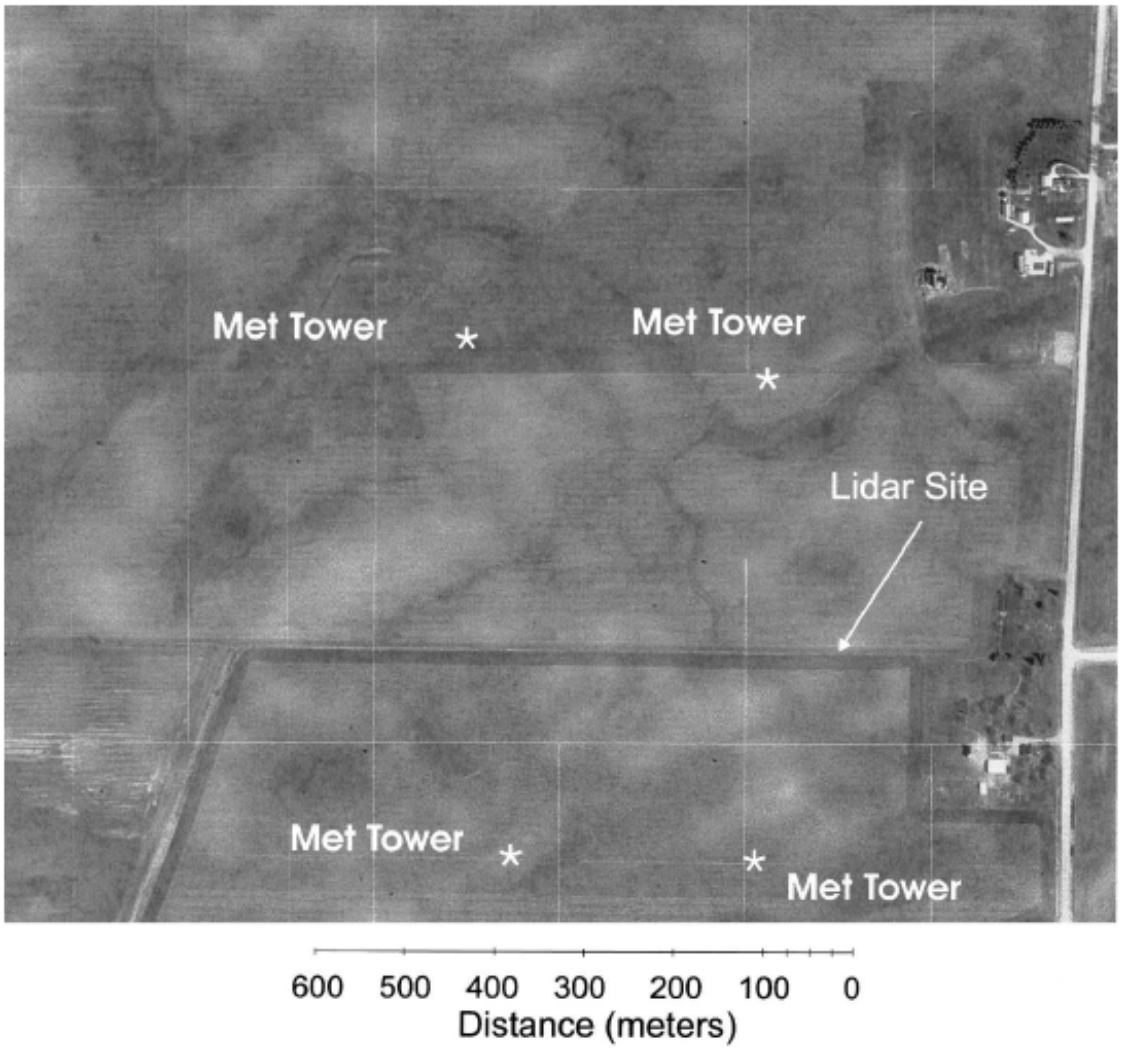

Figure 2. A black-and-white aerial photograph of the field campaign site showing a bare-soil condition. The vertically staring lidar was located at the boundary between a soybean field (south of (below) the lidar) and a cornfield (north of (above) the lidar). The boundary between the fields can be seen as a line. Higher elevation areas appear lighter in the photograph, while low areas are darker.

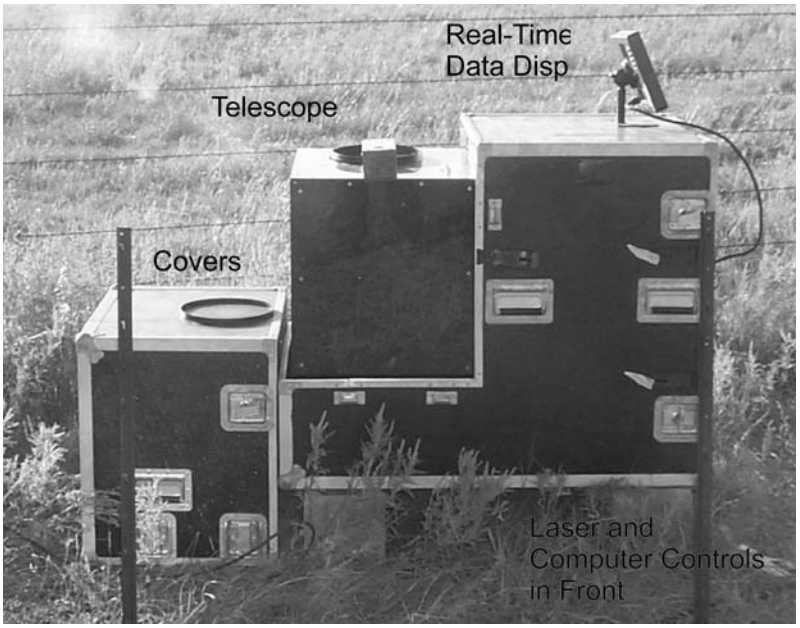

Figure 3. A photograph of the vertically staring elastic lidar. This system is highly compact and portable and requires no operator input once started.

The laser beam is emitted parallel to the axis of the receiving telescope at a distance of 24 cm from the center of the telescope. There is a minimum distance for which the lidar produces useful data. This is the distance at which the telescope images the entire laser beam, which is approximately 125 m for this lidar. Only that portion of the lidar signal that comes from the area of complete overlap between the field of view of the telescope and the laser beam can be reliably used for analysis.

A high-bandwidth (60 MHz) amplifier is located inside the detector housing. The signal is amplified as part of the detector system and fed to a 100-MHz, 12-bit digitizer on an IBM personal computer (PC)-compatible data bus. A computer is used to control the system and to take the data. The computer controls the system using high-speed data transfer to various cards mounted on the PC bus. This same multipurpose card is used to both set and measure the high voltage applied to the APD. The digitizers on the PC data bus are set

up for data collection by the host computer and start data collection on receipt of the start pulse.

Table 1. Operating characteristics of the vertically staring lidar system.

Transmitter		Receiver	
Wavelength	1064 or 532 nm	Type	Schmidt-Cassegrain
Pulse length	~10 ns	Diameter	0.254 m
Pulse repetition rate	50 Hz	Focal length	2.5 m
Pulse energy	125 mJ max	Filter bandwidth	3.0 nm
Beam divergence	~3 mrad	Field of view	1.0-4.0 mrad adjustable
		Range resolution	1.5, 2.5, 5.0, 7.5 m

The signal was collected with a vertical range resolution of 1.5 m, and 50 summed laser pulses per line of sight, for a time resolution of 1.08s. The data the lidar collected is related to the particulate concentration, which is used as a tracer of atmospheric motion. High particulate concentrations (shown in red in figure 4) are found near the surface. Lower concentrations (blues) are found near the top of the boundary layer where the air is cleaner. The clean air above the boundary layer is shown as white (uncolored). The plots of lidar data show the range resolved particulate concentration above the lidar as a function of time. The boundary between the particulate laden air and clean air above is taken to be the top of the boundary layer (Kovalev and Eichinger, 2004). Figure 4 is an example of three hours of lidar data.

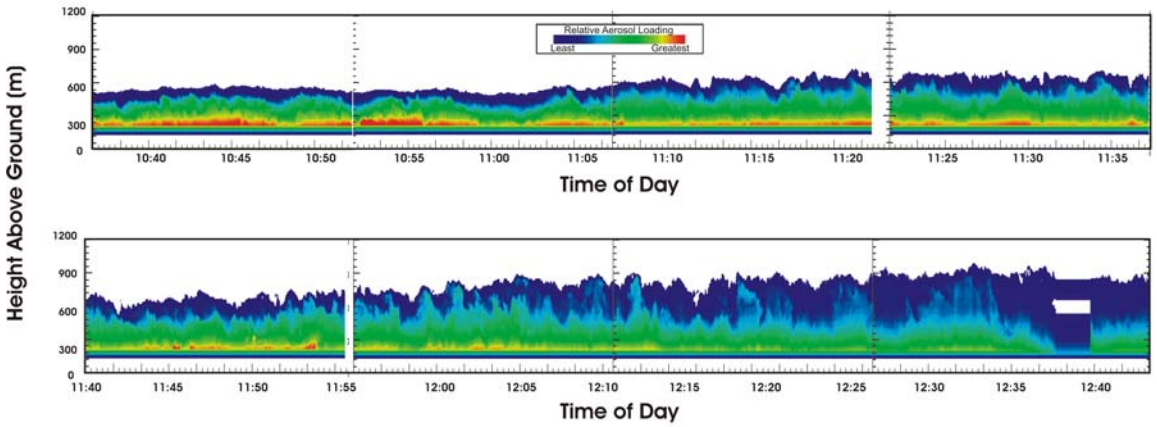

Figure 4. An example of two hours of lidar boundary layer data from 29 June, 2002. Red colors represent highest concentrations of particulates while greens and blues are lower. White areas at the top of the panels are the free troposphere.

CHAPTER 3

METEOROLOGICAL MEASUREMENTS

The temperature gradient of the lower atmosphere was obtained from standard Vaisala meteorological balloons launched at approximately 0700, 1000, 1400, and 1600 LST each day (Figure 7). The balloons were launched from the lidar location and monitored from there. The data from 27 June are shown in Figure 5, and are typical of the kind of boundary layers found during SMEX. The gradients were determined from the slope of the temperature data taken over four consecutive points, each about 20 m apart.

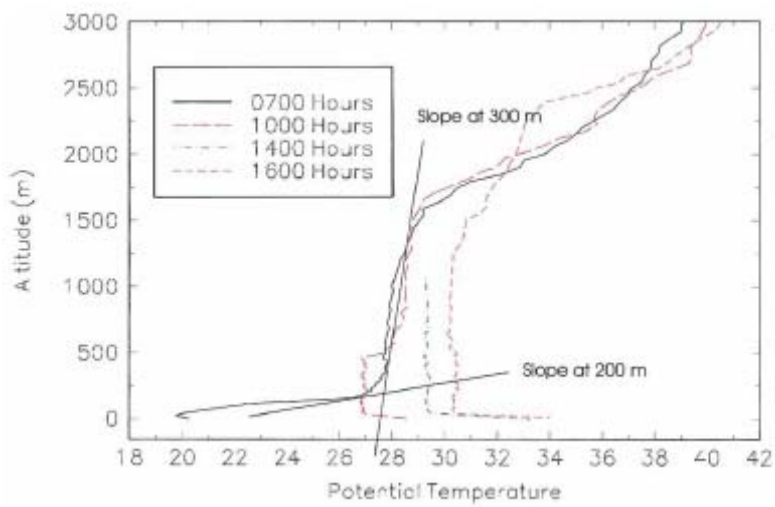

Figure 5. Radiosonde profiles from 27 Jun 2002. Also shown are the potential temperature gradients at 200 and 300 m for the 0700 LST flight. The large change in results in rapid growth of the boundary layer after it reaches the 300-m altitude.

The potential temperature profiles from the 0700 LST balloon data are characteristic of typical mornings in Iowa, from early June through the middle of September. Near the surface, the temperature rises with small

changes in height. In the section of the profile where the boundary layer is rapidly forming, there is little or no change in temperature with rising height. Above this region, the temperature rises with greater changes in height than are found below the formation of the boundary layer. Figure 6 shows the temperature gradients for June 25 and 29. The June 25 data has a pronounced area of boundary layer growth above 300m, while the June 29 data shows a more constant temperature gain with rising height.

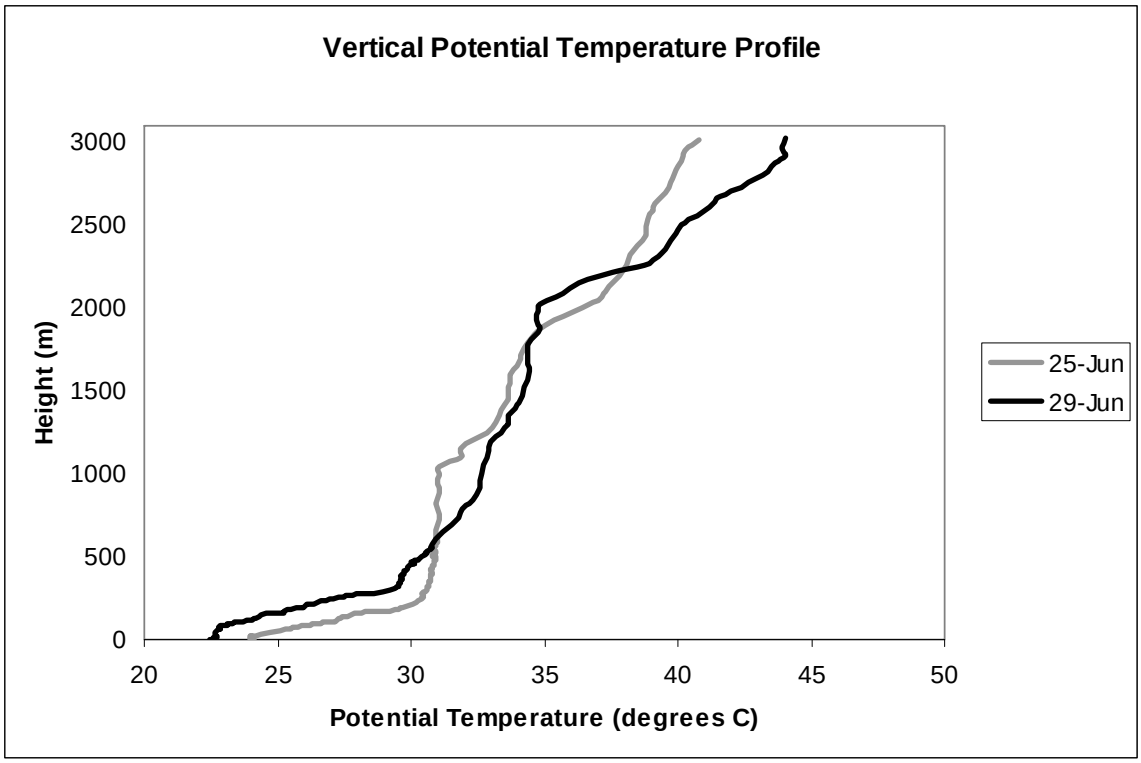

Figure 6 – June 25, 2002, 0658 and June 29, 0707.

Meteorological balloons only provide measures every few meters, with decreasing frequency as the balloon rises, and although potential temperature is generally expected to rise or remain constant with height, it is

not uncommon for some of the successive temperature readings to decrease between individual measurements, resulting in a negative temperature gradient. Calculating temperature gradients over four points limits the occurrence of negative values and provides a temperature gradient that is more representative of the gradient around the entrainment zone, which can span several hundred meters. Also, since there is no temperature reading for every meter of height, calculating the gradient over several points provides an average to correspond with any measurement of boundary layer height. If the temperature gradient was averaged over too many points, the profile would have a more uniform slope and the three regions of the profile shown in Figures 5 would be less defined.

The sensible heat fluxes that were used for reference were obtained from four CSAT3 sensors (Campbell Scientific 3-D sonic anemometer) each collocated with a LI7500 (Li-Cor CO_2/H_2O analyzer) using the eddy covariance method (Figure 8). These systems provide high frequency (20 Hz) data of wind (*u*, *v*, and *w* components), sonic temperature (*TS*), water vapor and CO_2. Two of the instruments were placed in the cornfield and two in soybeans within 600 m of the lidar location. A Libretto (Toshiba) mini computer was used to store all of the raw high frequency data in "time series mode" so that it could be processed offline. The high frequency eddy covariance data (20 Hz) were processed to apply the recommended manufacturers' scan offset corrections, to apply a 2-D coordinate transformation that forces v = w = 0 (Kaimal and Finnigan, 1994) and to correct for oxygen and density effects on the evaporative and CO_2 fluxes (Webb-Pearman-Leuning-WPL correction; Webb et al., 1980). The data was also adjusted to close the energy balance based upon the measured Bowen ratio.

Figure 7. A photograph of SMEX field campaign team members launching a Vaisala meteorological balloon.

Figure 8. A photograph of the CSAT3 and LI7500 station.

CHAPTER 4

LIDAR DATA ANALYSIS METHODOLOGY

Potential temperature and specific humidity profiles are most often used to estimate the height of the boundary layer. This height is taken to be the height at which the potential temperature is subject to an abrupt increase. A similar decrease in the specific humidity (and all other scalar quantities whose sources are at the surface) occurs at the same height. A fair-weather, convective boundary layer is characterized by warm, particulate-rich parcels of air rising from the surface, and cooler, cleaner parcels of air moving toward the surface. From elastic lidar data, the top of the convective boundary layer is marked by a sharp contrast between the backscatter signals from particulate-rich structures below and cleaner air above (Figures 1 and 9). Because the lidar data are sampled approximately every second, a considerably higher temporal resolution than that of a balloon, the determination of the height of the boundary layer and thickness of the entrainment zone is more complex.

Given that the height of the boundary layer can be determined for each of the individual lidar scans, for a half-hour period there will be a set of approximately 1800 separate height measurements. There is, thus, a distribution of heights rather than a single height as might be measured by a balloon. The height of the boundary layer is taken to be the arithmetic mean of the individual heights in this set. The entrainment zone thickness (EZT) was defined by Deardorff et al. (1980) as "the depth being confined between the outermost height reached by only the most vigorous penetrating parcels and by the lesser height where the mixed-layer fluid occupies usually some

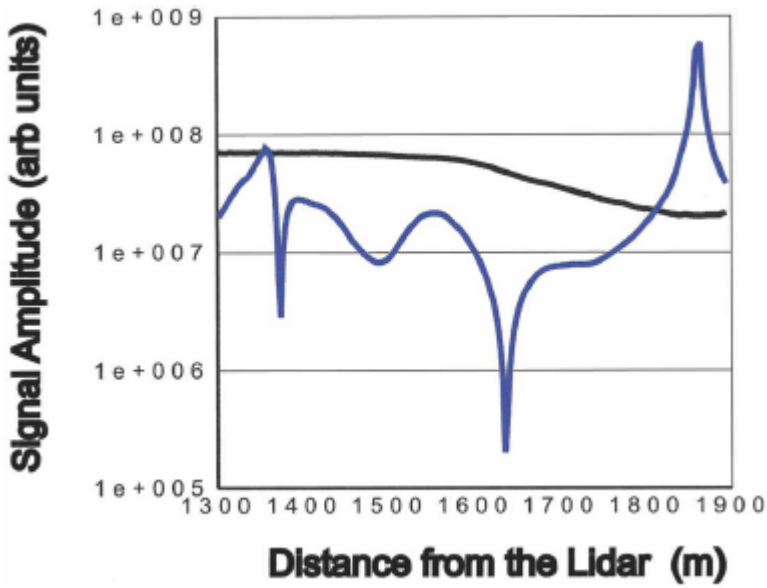

Figure 9. An example of a lidar scan showing the top of the boundary layer and the values for the edge-detection function (blue line), and the lidar signal showing the decrease in aerosol concentration at the top of the boundary layer (solid line). The value of the edge detection function shows a sharp decrease at inflection points.

90 to 95 percent of the total area." Many of the lidar- based methods to determine the EZT use the standard deviation σ of the set of boundary layer heights in a given period of time as a measure of the EZT. Then, the bottom of the boundary layer, where the mixed-layer fluid occupies 95% of the total area, is that height for which 5% of the measured boundary layer heights in the set are below. For example, Steyn et al. (1999) estimate the EZT=2.77σ (i.e., $h_{top} = h + 1.38\sigma$ and $h_{bottom} = h - 1.38\sigma$), corresponding to 8%–92% of the total variation in heights. Melfi et al. (1985) used a nonsymmetric cutoff in which the bottom of the entrainment zone h_{bottom} corresponded to a cumulative probability of 4%, while h_{top} corresponded to a cumulative probability of 98%. This study uses h_{top} = 95th percentile and h_{bottom} = 5th percentile, similar to those suggested by Deardorff et al. (1980). The

estimates of A can be considerably different, depending upon the values used for the cutoff. The difference between assuming the mixed-layer fluid occupies 92% versus 95% of the total area can lead to a difference of approximately 20% in A. A detailed description of various methods for the determination of boundary layer height and entrainment zone thickness from lidar data can be found in Kovalev and Eichinger (2004).

The height of the boundary layer for an individual lidar scan is found using an edge-detection method originally developed for digital photography (Davies 1992). The method determines, at each point, the absolute value of the second derivative of the lidar signal with respect to altitude divided by the first derivative of the lidar signal with respect to altitude. The minimum of this function is a sensitive indicator of the cusp in the lidar signal where the sign of the second derivative changes sign. This point is generally midway between the high-particulate levels that are indicative of the boundary layer and the lower levels that are indicative of the free troposphere, and is taken to be the height of the boundary layer. Extended derivatives are used to calculate the derivatives to minimize the effects of noise in the lidar signal. The derivatives are extended over a distance of 20 points on either side of the point in question. Figure 9 is an example of a lidar scan showing the top of the boundary layer and the values for the edge detection function. The height of the boundary layer is defined by the upwelling parcels of air that rise from the surface and the downwelling parcels of air from above (see, e.g., Figure 1). The passage of each of these upwelling and downwelling parcels of air provides a wide range of height measurements that define the top and bottom of the EZT. The greater the amount of these events that can be measured, the better the estimate of the EZT and h will be. The number of these that can be measured by a vertically pointing lidar depends on the time required for an

upwelling parcel of air to drift over the lidar, and, thus, the wind speed. Assuming 4 ms^{-1} wind speed and a 1-km horizontal scale for a large parcel, a parcel of air will take about 6 minutes to pass over the lidar. As is often the case with nonstationary atmospheric measurements, there are competing demands for sufficient measurements to capture all of the spectral modes and the need to limit the data collection time so that the average does not change appreciably. Averaging over enough plumes to obtain statistically meaningful boundary layer heights may take too long during times when the height is changing rapidly (e.g., during midmorning or late afternoon). For this study, 30-min averages were used, in part because it is a commonly used averaging period for surface fluxes and was the averaging period used in SMACEX. This time is occasionally too long during periods when the boundary layer grows rapidly. The boundary layer heights and EZTs for 15-min periods were determined for this study.

CHAPTER 5
DISCUSSION

Using the lidar data processed as described above, *A* values were calculated over 15-minute increments from approximately 0700-1200 for the experimental period (23, 25, 27 and 29 June) using Eq. (3). The days chosen are similar fair-weather days with both lidar and balloon data available. The corresponding temperature gradient for each value of *A* was determined based on boundary layer height. There is little that can be inferred from a direct comparison between the calculated *A* values and the corresponding temperature gradients, see Figure 10. Although the calculated values of the entrainment parameter vary greatly from the accepted value of 0.2, for any given temperature gradient, there are a number of corresponding values for the entrainment parameter. In an extensive examination of the various estimates of the entrainment parameter, Beyrich (1994; 1995) showed that the differences in suggested values for *A* resulted in significant differences in the height of the boundary layer and other derived parameters. A similar result was achieved by Nelson, Stull, and Eloranta (1989, hereafter Nelson et al 1989) when they investigated the relationship between the entrainment rate and entrainment zone thickness.

Nelson et al (1989) tested several published diagnostic relationships for entrainment zone thickness using data from ground based lidar. Several conflicting relationships were achieved, yet all were supported by the experimental data. It was found that the results of the various diagnostic relationships were not in conflict when they were viewed as a function of time. Figure 11 is a copy of a plot of the normalized EZ depth vs. normalized entrainment rate produced by Nelson et al (1989). Several of the power law

diagnostic relationships tested are shown as tangent to the curve. This figure demonstrates that for any given value of entrainment rate, there are multiple possibilities for EZ thickness, depending on time, or more appropriately the time evolution of boundary layer development. In order to establish a more conclusive relationship between the entrainment parameter and the vertical temperature gradient, the individual points must be displayed in relation to the time evolution of the boundary layer.

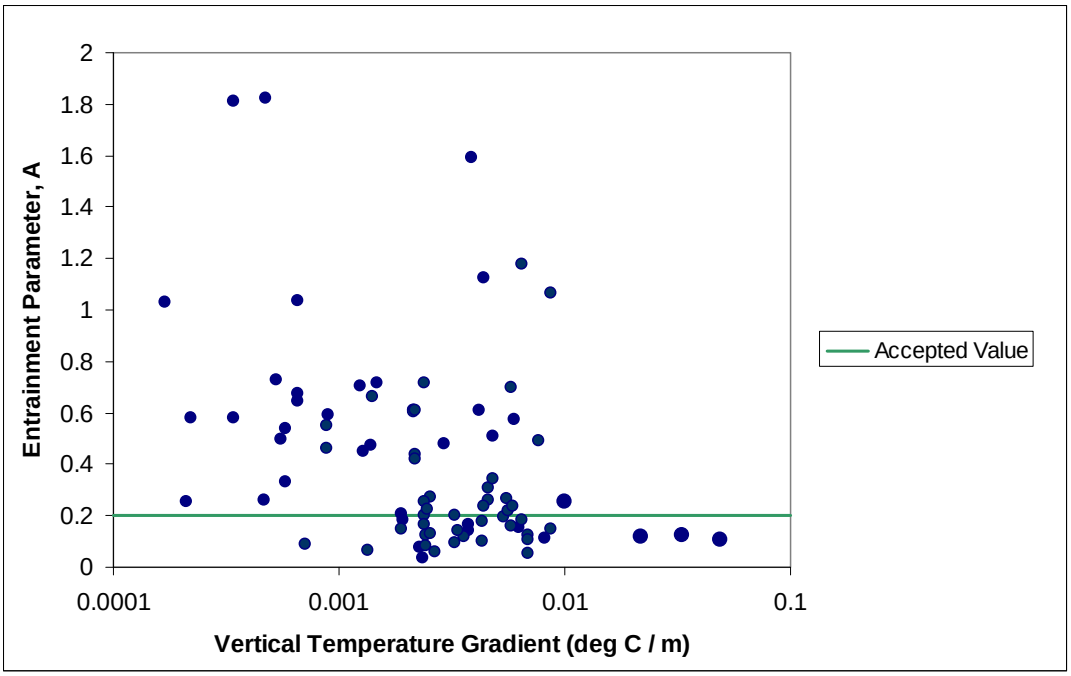

Figure 10. The calculated values of the entrainment parameter *A* are plotted against the vertical potential temperature gradient corresponding to boundary layer height. The commonly accepted value of A=0.2 is plotted as a line.

In Chapter 3, we introduced the temperature profiles for the experimental period and discussed how the profile is divided into three regions based on boundary layer development. On a day with fair-weather conditions and

minimal advection, the mixed layer follows a typical three-stage evolution (Stull 1988). In the early morning, the shallow mixed layer rises slowly as the nocturnal stable layer dissipates. This results in a large change in temperature for the first 200 to 300 meters of the temperature profile. By late morning, 1000-1200 Central Daylight Time (CDT), the mixed layer rises rapidly through the previous day's weakly stable residual layer. This corresponds to the portion of the temperature profile where rapid boundary layer growth occurs. In this region, the change in temperature with height is close to zero. Finally, the mixed layer top grows until it reaches the previous day's capping inversion, resulting in a quasi-steady deep convective boundary layer (Nelson et al 1989). Above this point, the temperature changes steadily with height.

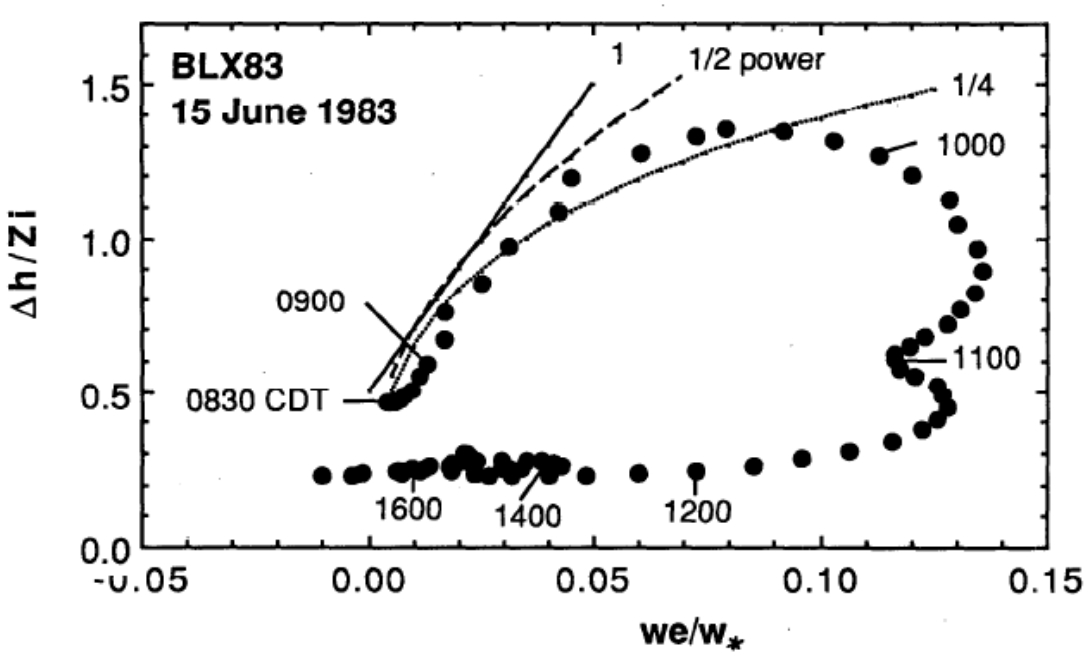

Figure 11. Figure 5 from Nelson et al (1989) showing the evolution of normalized entrainment zone depth (Δh) with entrainment velocity (w_e) for 15 June 1983 at the BLX83 field site in Oklahoma. Power law relationships (offset in the vertical for easier comparison with the data points) are also sketched.

Based on the concept of three stage boundary layer evolution, the A values calculated for each of the four dates were divided into three groups. Classification of the data into the three groups is dependent on where the corresponding boundary layer height is located compared to the three stages of the temperature profile, an example of this classification is shown in Figure 12. The A values and corresponding boundary layer heights for each date were related to the balloon data for the same day, except in the case of June 23. There is no 0700 balloon data for June 23. The only balloon available for that date was launched after 1200, when lidar data was no longer being collected. Since the four experiment days were similar fair-weather days, the data for June 23 was divided using the other three early morning temperature profiles. In classifying the values of the entrainment parameter A into the three stages of boundary layer growth, we can now examine a prognostic behavior with time when plotted against the vertical temperature gradient (see Figure 13). This finding is consistent with previous work by Nelson et al (1989), in which a hysteresis behavior with time was established for normalized entrainment zone depth plotted against entrainment velocity.

Starting in the mornings with weak convection, near zero entrainment and a strong capping nocturnal inversion (at approximately 0830 CDT), Nelson et al (1989) found the entrainment zone thickness to be on the order of 0.5 to 0.8 times the average mixed layer depth. From Eq. (3):

$$A = \frac{EZT}{2h - EZT} = \frac{0.5h}{2h - 0.5h} = 0.3$$

This part of the evolution corresponds to the portion of the potential temperature gradient where the temperature increases the greatest with height, dT/dH > 0.01. For this study, the values of *A* which correspond to this portion of the temperature gradient range from 0.1 – 0.25 and are shown in Figure 13 as diamonds. The entrainment coefficient is small during the early morning due to the slow growth of the mixed layer and near zero entrainment.

Later in the morning (between about 0900 and 1000 CDT) the entrainment rate increases and the capping nocturnal inversion weakens. At this time, the surface sensible heat flux has increased dramatically and the strength of

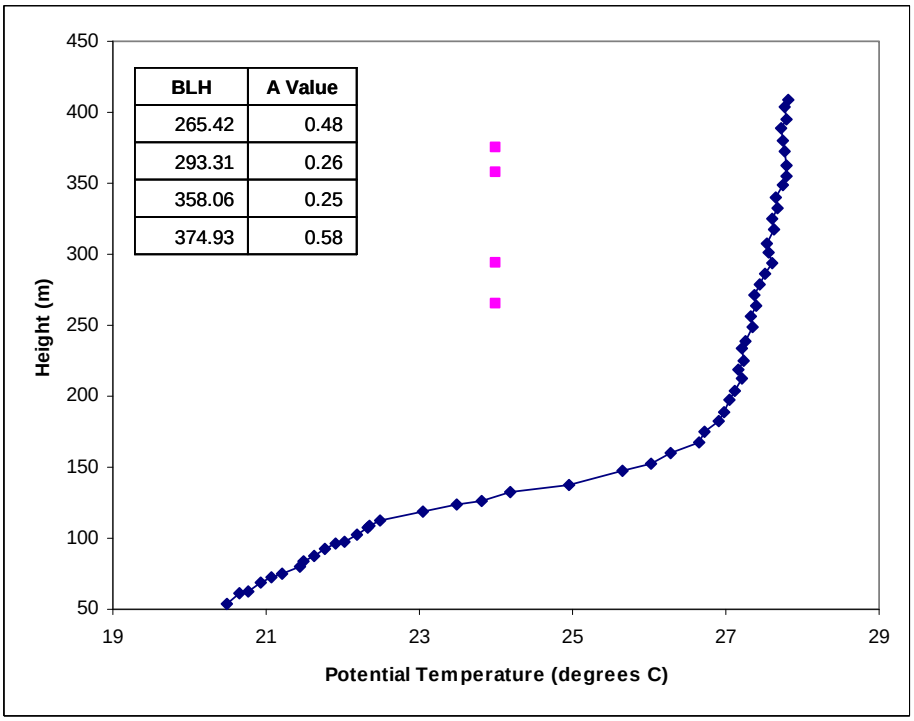

Figure 12. A sampling of the June 27 temperature profile showing two distinct regions of boundary layer development close to the earth's surface. A sampling of boundary layer heights and corresponding values of *A* for the same date fall within the region of the temperature profile where rapid boundary layer growth occurs.

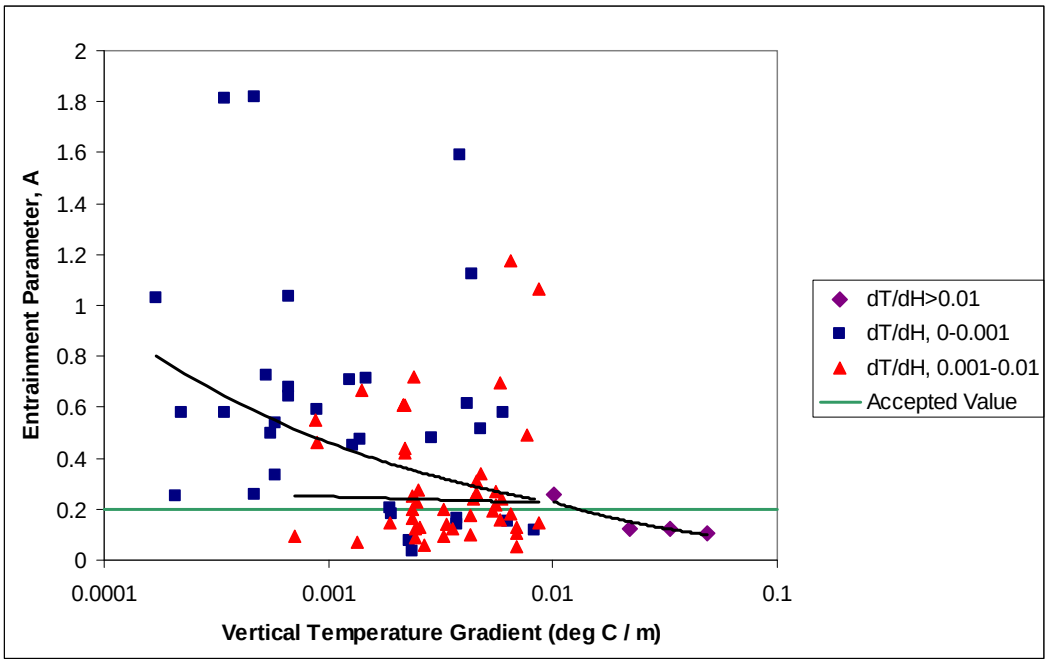

Figure 13. The calculated values of the entrainment parameter A are plotted against the vertical temperature gradient. In this graph, the data points have been divided into three groups based on the temperature profile. The commonly accepted value of 0.2 is plotted as a line, so are the trendlines associated with each of the three groups of data.

the capping inversion has decreased (the potential temperature gradient decreases). The result is a period of dramatic growth in the height of the boundary layer. Nelson et al (1989) found that the EZ depth increases to its maximum thickness of about 0.8 to 1.5 times the average mixed layer depth. Using Eq. (3):

$$A = \frac{EZT}{2h - EZT} = \frac{1h}{2h - 1h} = 1$$

During this time, the potential temperature gradient is very small, the temperature is near constant with rise in height, dT/dH lies primarily

between 0 and 0.001. Calculated *A* values during this period of boundary layer growth show a much broader range than the 0.1-0.3 which is widely accepted (Figure 13), averaging approximately 0.6, with some values reaching as high as 1.8. During this period of rapid boundary layer growth, the contribution to the growth of the boundary layer from the entrainment of free atmosphere air approaches the contribution from rising thermals. This is to be expected given that smaller changes in temperature with altitude result in greater penetration of the warm parcel rising from below. This is also consistent with the unusually deep entrainment zone observed by Nelson et al. (1989) and suggests that 0.2 is not an appropriate value to use for the entrainment coefficient during the period in which the boundary layer is rapidly growing.

By mid- to late morning (1000 – 1100 CDT), the EZ thickness begins to decrease. During the period of rapid ML rise through the residual layer, the EZ thickness is about 60%-70% of its earlier maximum thickness. Between about 1000 and 1200 CDT, both the EZ thickness and the entrainment rate smoothly decrease, as the ML reaches the strong capping inversion remaining from the previous day's mixed layer. For much of the afternoon, there is virtually no entrainment, and the EZ thickness is a nearly constant 15% - 25% of the average ML depth (Nelson et al 1989). The temperature gradient in this area shows a steady change in temperature with height, dT/dH lies between 0.001 and 0.01 and calculated *A* values occur frequently in the range of 0.1 – 0.3, though some reach much higher. These higher values correspond to the period of rapid ML rise through the residual layer described by Nelson et al (1989).

A limitation of the simple constant *A* approach is that it ignores the essentially dynamic character of the entrainment process. During the time

when boundary layer theory was being developed, it was often suggested that the value would change with different conditions (Carson,1973; Betts and Barr, 1997) Indeed, one of the first to outline a theory of the boundary layer suggested that A might change as the boundary layer evolves (Carson, 1973). Based on the best fit lines shown on the graph in Figure 13, one could select an appropriate value to use for the entrainment parameter if the temperature profile is available. For temperature gradients between 0.01 and 0.1, when the BLH measurement falls in the first 200-300 meters of the atmosphere where the temperature gradient is very flat (early in the morning), an entrainment coefficient A in the range of 0.1 – 0.25 is appropriate. For temperature gradients between 0 and 0.01, when the BLH measurement falls in the mid-morning region of rapid boundary layer growth, the curve ranging from 0.25 and 0.8 provides a good estimate. During the late morning and early afternoon, when boundary layer growth slows and the temperature profile shows a nearly constant rise in temperature with rise in height between 0.001 and 0.01, $A = 0.25$ should be used.

CONCLUSION

In the Batchvarova–Gryning model and other boundary layer height models which use the entrainment coefficient A to account for the entrainment of free atmosphere air into the boundary layer, the value is taken to be a parameter of constant value, typically in the range of 0.1-0.3, with 0.2 as the widely accepted average (Stull 1976). Since the value of the entrainment parameter represents the ratio of the virtual potential temperature fluxes at the surface and at the top of the boundary layer (Stull 1988), errors in the estimation of the parameter result in errors in the amount and rate of boundary layer growth, an important parameter in many applications (for example, the mixing of pollutants emitted into the atmosphere). For situations in which the boundary layer is growing rapidly, and the value of A is much larger than 0.2, the rate of growth can be in error by as much as a factor of 3, with the result that other calculated parameters may be significantly in error.

The results obtained here indicate that during some periods of boundary layer growth, the entrainment coefficient does not maintain a constant value. It is a characteristic that changes depending on the stages of boundary layer evolution. In order to investigate these concepts further, more data is required. Additional boundary layer measurements for similar fair-weather days to those experienced during the SMEX field campaign would provide more calculated values of A with which to draw conclusions from. For future experiments, balloon data should be gathered with greater frequency, in order to relate the boundary layer growth with the real-time temperature profile. At a minimum, balloons should be launched at 0830, 0900, 1000, 1100 and 1200 in order to provide temperature profiles at all of the key

stages of boundary layer development. This study is limited in that it only examines the value of the entrainment parameter for one climate condition in one geographic region. There is an opportunity to expand the study to other types of weather (i.e. windy days) and geographic regions outside of the Midwest.

REFERENCES

Angevine, W.M., 1999. Entrainment results with advection and case studies from the Flatland boundary layer experiments. *Journal of Geophysical Research*, 104, 30947-30963.

Batchvarova, E., Gryning, S.E., 1991. Applied model for the growth of the daytime mixed layer. *Boundary-Layer Meteorology,* 56, 261-274.

Batchvarova, E., Gryning, S.-E., 1994. Applied model for the height of the daytime mixed layer and the entrainment zone. *Boundary-Layer Meteorology,* 71, 311-323.

Betts, A.K., 1973. Non-precipitating cumulus convection and its parameterisation. *Quarterly Journal of the Royal Meteorological Society,* 99, 178-196.

Betts, A.K., 1992. FIFE atmospheric boundary layer budget methods. *Journal of Geophysical Research,* 97, 18523-18531.

Betts, A. K., Ball F.K., 1994. Budget Analysis of FIFE 1987 Sonde Data. *Journal of Geophysical Research*, 99, 3655-3666.

Betts, A. K., Ball F.K., 1995. The FIFE Surface Diurnal Cycle Climate. *Journal of Geophysical Research*, 100(D12), 25679-25693.

Betts, A. K., Ball F.K., 1998. FIFE Surface Climate and Site-Averaged Data Set 1987-1989. *Journal of Atmospheric Science*, 55, 1091-1108.

Betts, A. K., Barr, A.G., 1987. First International Satellite Land Surface Climatology Field Experiment Sonde Budget Revisited. *Journal of Geophysical Research*, 101, 23285-23288.

Betts, A.K., Barr, A.G., 1997. First international satellite land surfaces climatology Field Experiment 1987 sonde budget revisited. *Journal of Geophysical Research,* 101, 23,285-23,288.

Betts, A. K., Desjardins, R.L., MacPherson, J.I., 1992. Budget Analysis of the Boundary Layer Grid Flights during FIFE 1987. *Journal of Geophysical Research*, 97, 18533-18546.

Betts, A. K., Desjardins, R.L., MacPherson, J.I., Kelly, R.D., 1990. Boundary Layer Heat and Moisture Budgets from FIFE. *Boundary-Layer Meteorology*, 50, 109-137.

Beyrich, F., 1994a. Sodar observations of the stable boundary layer height in relation to the nocturnal low-level jet. *Meteorologische Zeitschrift (N.F.)*, 3, 29-34.

Beyrich, F., 1994b. Bestimmung der Mischungsschichthohe aus Sodar-Daten unter Verwendung numerischer Modellrechnungen. Frankfurt/M.: Wiss.-Verlag Dr. W. Maraun (ISBN 3-927548-67-7). Schriftenreihe des FhI fu r Atmospharische Umweltforschung Garmisch-Partenkirchen Bd. 28, 161 pp. + Appendix.

Beyrich, F., 1995. Mixing height estimation in the convective boundary layer using sodar data. *Boundary-Layer Meteorology,* 74, 1-18.

Carson, D.J., 1973. The development of a dry inversion-capped convectively unstable boundary layer. *Quarterly Journal of the Royal Meteorological Society,* 99, 450-467.

Clarke, R.H., 1990. Modeling mixed layer growth in the Koorin experiment. *Australian Meteorological Magazine,* 38, 227-234.

Culf, A., 1992. An application of simple models to Sahelian convective boundary layer growth. *Boundary-Layer Meteorology,* 58, 1-18.

Davies, E.R., 1992. A Skimming technique for fast accurate edge detection. *Signal Processing*, 26, 1-16.

Davies, K.J., Lenschow D.H., Oncley, S.P., Kiemle, C., Ehret, G., Giez, A., Mann, J., 1997. Role of entrainment in surface-atmosphere interaction over the boreal forest. *Journal of Geophysical Research*, 102(D24), 29219-29230.

Deardorff, J.W., Willis, G.E., and Stockton, B.H., 1980. Laboratory studies of the entrainment of a convectively mixed layer. *Journal of Fluid Mechanics*, 100, 41-64.

Driedonks, A.G.M., 1982a. Sensitivity analysis of the equations for a convective mixed layer. *Boundary-Layer Meteorology,* 22, 475-480.

Driedonks, A.G.M., 1982b. Models and observations of the growth of the atmospheric boundary layer. *Boundary-Layer Meteorology*, 23, 283-306.

Eichinger, W.E., Holder, H.E., Cooper, D.I., 2005. Lidar Measurement of Boundary Layer Evolution to Determine Sensible Heat Fluxes. *Journal of Hydrometeorology*, 6, 840-1027.

Gryning, S.-E., Batchvarova, E., 1990. Analytical model for the growth of the coastal internal boundary layer during onshore flow. *Quarterly Journal of the Royal Meteorological Society*, 116, 187-203.

Gryning, S.-E., Batchvarova, E., 1994. Parametrization of the depth of the entrainment zone above the daytime mixed layer. *Quarterly Journal of the Royal Meteorological Society*, 120, 47-58.

Kailstrand, B., Smedman, A.S., 1997. A case study of the near-neutral coastal internal boundary layer growth: Aircraft measurements compared with different model estimates. *Boundary Layer Meteorology*, 85, 1-33.

Kovalev, V., Eichinger, W., 2004. *Elastic Lidar: Theory, Practice and Analysis Methods*. Wiley and Sons, New York.

Kustas, W., Hatfield, J., Prueger, J., 2005. The soil moisture atmosphere coupling experiment (SMACEX): Background, hydrometeorological conditions and preliminary findings. *Journal of Hydrometerology*, 791-804.

Mahrt, L., Lenschow, D.H., 1976. Growth Dynamics of the Convectively Mixed Layer. *Journal of Atmospheric Science*, 33, 41-51.

Margulis, S., Entekhabi, D., 2003. Variational assimilation of radiometric temperature and reference level micrometeorology into a model of the atmospheric boundary layer and land surface. *Monthly Weather Review*, 131, 1272-1288.

Melas, D., Kambezidis, H. D., 1992. The Depth of the Internal Boundary Layer over an Urban Area under Sea-Breeze Conditions. *Boundary-Layer Meteorology*, 61, 247-274.

Melfi, S. H., Spinhirne, J. D., Chou, S. H., and Palm, S. P., 1985. Lidar observation of vertically organized convection in a planetary boundary layer over the ocean. *Journal of Climate Applied Meteorology*, 24, 806-821.

Nelson, E., Stull, R., Eloranta, E., 1989. A Prognostic Relationship for Entrainment Zone Thickness. Journal of Applied Meteorology, 28, 885-903.

Nicholls, S., LeMone, M.A., 1980. The fair weather boundary layer in GATE: The relationship of subcloud fluxes and structure to the distribution and enhancement of cumulus clouds. *Journal of Atmospheric Science*, 37, 2051-2067.

Seibert, P., Beyrich, F., Gryning, S.E., Joffre, S., Rasmussen, A., Tercier, P., 1998. Mixing layer depth determination for dispersion modelling. European Commission. In: Fisher, B.E.A., Erbrink, J.J., Finardi, S., Jeannet, P., Joffre, S., Morselli, M.G., Pechinger, U., Seibert, P., Thomson, D.J. (Eds.), 1998: COST Action 710-Final Report. Harmonisation of the pre-processing of meteorological data for atmospheric dispersion models. L-2985 Luxembourg: European Commission, EUR 18195 EN (ISBN 92-828-3302-X).

Smeda, M. S., 1979. A Bulk Model for the Atmospheric Planetary Boundary Layer. *Boundary Layer Meteorology*, 17, 411-427.

Steyn, D. G., Baldi, M., and Hoff, R. M., 1999. The detection of ixed layer depth and entrainment zone thickness from lidar back-scatter profiles. *Journal of Atmospheric Oceanic Technology*, 16, 953-959.

Stull, R.B., 1976a. The energetics of entrainment across a density interface. *Journal of the Atmospheric Sciences*, 33, 1260-1267.

Stull, R.B., 1976b. Internal gravity waves generated by penetrative convection. *Journal of the Atmospheric Sciences*, 33, 1279-1286.

Stull, R.B., 1988. *An Introduction to Boundary Layer Meteorology*. Kluwer Academic Publishers, Dordrecht, 665 pp.

Tennekes, H., 1973. A model for the dynamics of the inversion above a convective boundary layer. *Journal of the Atmospheric Sciences,* 30, 558-567.

Tennekes, H., van Ulden, A.P., 1974. Short term forecasts of temperature and mixing height on sunny days. *Proceedings of Second AMS Symposium Atmospheric Diffusion & Air Pollution, Santa Barbara*, pp. 35-40.

Yamada, T., Berman, S., 1979. A critical evaluation of a simple mixed layer model with penetrative convection. *Journal of Applied Meteorology*, 18, 781-786.

Zilitinkevich, S.S., 1972. On the determination of the height of the Ekman boundary layer. *Boundary-Layer Meteorology*, 3, 141-145.

Zilitinkevich, S.S., 1975. Comments on a paper by H. Tennekes. *Journal of the Atmospheric Sciences,* 32, 991-992.